Measurements of the structure of the Reynolds stress in a turbulent boundary layer

By S. S. LU AND W. W. WILLMARTH

Department of Aerospace Engineering, The University of Michigan

Additional experimental studies of the structure of Reynolds stress which supplement our previous work (Willmarth & Lu 1971) are reported. The velocity at the edge of the viscous sublayer is again used as a detector signal for bursts and sweeps. The signal uv obtained from an X-wire probe at various locations is conditionally sampled and sorted into four quadrants of the u, v plane. Using this method it is found that, when the velocity u_w at the edge of the viscous sublayer becomes low and decreasing, a burst occurs. On the other hand, a sweep occurs when u_w becomes large and increasing. The convection speeds of the bursts and the sweeps are found to be equal and are about 0·8 times the local mean velocity and 0·425 times the free-stream velocity at a distance $y \simeq 0.15\delta^*$ from the wall (δ^* is the displacement thickness). Throughout the turbulent boundary layer, the bursts are the largest contributors to $\overline{uv}$ with the sweeps the second largest. On average, the bursts account for 77 % of $\overline{uv}$, while the sweeps provide 55%; the excess percentage over 100 % is due to the other small negative contributions.

Characteristic mean time intervals are obtained for both bursts and sweeps from certain unique features of the measurements of fractional contributions to $\overline{uv}$ from different events. Both mean time intervals are approximately equal and constant for most of the turbulent boundary layer. The scaling of the mean time interval between bursts with outer flow variables is confirmed. It is suggested that many of the features of the fluctuating flow revealed by the measurements may be explained by convection past the measuring station of an evolving deterministic flow pattern such as the hairpin vorticity model of Willmarth & Tu (1967).

1. Introduction

In a previous paper Willmarth & Lu (1971) reported conditionally sampled measurements of the structure of the Reynolds stress at a single point very near a wall. The present paper describes a more detailed and complete set of measurements of the structure of the Reynolds stress throughout the boundary layer. These measurements, like those in the above paper, were guided by knowledge accumulated from the numerous visual observations of the flow structure of the boundary layer during the bursting process.

These visual observations of Kline et al. (1967), Kim, Kline & Reynolds (1968,

1971), Corino & Brodkey (1969) and Grass (1971) were discussed by Willmarth & Lu (1971) and will not be described again in this paper. Recently, a number of additional quantitative results have been obtained from hot-wire or hot-film measurements of Reynolds stress and/or bursting phenomena. These results have appeared in the papers of Blackwelder & Kaplan (1971), Wallace, Eckelmann & Brodkey (1972), Rao, Narasimha & Badri Narayanan (1971) and Gupta & Kaplan (1972). We shall mention and discuss these new results as we describe our own measurements in the main body of the paper.

The paper begins with a discussion of measurements of the spatial scale and convection of the organized bursting structure. This is followed by measurements of uv throughout the boundary layer in which the outward flow of fluid with low streamwise momentum is shown to contribute more to the Reynolds stress than does the inward flow of fluid with high streamwise momentum. This is followed by critical examination of methods and measurements used to determine the mean time between bursts and sweeps. We have also measured the mean duration of bursts and sweeps. The paper is a summary of the doctoral dissertation of S. S. Lu (Lu & Willmarth 1972). A copy can be obtained from the senior author at no charge until the present supply is exhausted.

2. Experimental apparatus and methods

The experiments were conducted in a thick ($\delta \simeq 5$ in.) turbulent boundary layer in the 5×7 ft wind tunnel of the Department of Aerospace Engineering at the University of Michigan. Most of the measurements were done in a boundary layer with a thick sublayer that was produced at low free-stream speeds $U_\infty \simeq 20$ ft/s. A few measurements were made at higher free-stream speeds $U_\infty \simeq 200$ ft/s.

A complete description of the experimental apparatus has been given in Willmarth & Lu (1971). This includes the mean flow in the boundary layer, the hot-wire probes, the electronic equipment and the analog-to-digital converter used to prepare the data from the low-speed boundary layer for digital processing. In the present work the same apparatus was used for the bulk of the measurements at low mean speeds $U_\infty \simeq 20$ ft/s. At high speeds $U_\infty \simeq 200$ ft/s, we again used the same equipment with the exception that the analog-to-digital conversion was performed using a Raytheon Model DM-120 multiplexer, a Raytheon Model AD-10A analog-to-digital converter, an IBM 729II Digital Magnetic tape unit and a Raytheon Format generator. This equipment was capable of 21 000 s^{-1}, 6 bit, analog-to-digital conversions per channel, i.e. (± 3 % accuracy). The input data were originally recorded in analog form using an FM tape recorder and were reproduced, for conversion to digital form, at one-eighth of the original speed. The bandwidth of the digitized data extends to frequencies of order 16·8 kHz (assuming that 10 digital conversions are required per period for reasonably accurate identification of single events). The data reduction was done with an IBM 360/67 computer using several simple FORTRAN programs and a few assembly language subroutines. We emphasize that the use of the digital computer for data reduction makes it possible to measure a great variety of

different statistical parameters inexpensively and efficiently. Indeed, we could not have performed all the measurements using analog methods, owing to imitations on time and money.

3. Conditionally sampled measurements of Reynolds stress

The method of conditional sampling was first used by Kibens (1968) (see Kovasznay, Kibens & Blackwelder (1970) for a summary) in a study of the motion and shape of the turbulent bulges in the outer intermittent region of a turbulent boundary layer. The concepts of conditional sampling were extended by Willmarth & Lu (1971) in a study of the structure of the Reynolds stress near the wall. The fluctuating streamwise velocity u_w (lower-case letters refer to fluctuating velocity components with zero mean) at the edge of the sublayer provided the detector signal. Willmarth & Lu (1971) found that, when u_w became low and decreasing, a burst occurred. They also found that the signal u_w when passed through a low-pass filter provides better criteria for identification of samples of uv that contribute to the Reynolds stress when u_w decreases. Thus, it was decided to use the filtered† fluctuating streamwise velocity u_w at the edge of the sublayer as the detector signal in the present study.

The spatial distribution of the Reynolds stress was studied using the same conditional sampling method as that employed by Willmarth & Lu (1971). However, the sampled Reynolds stress in the present paper is further sorted according to the different events involved. Thus, the spatial distribution and decay of the different events can be investigated from these sampled and sorted Reynolds stresses.

3.1. *Method of measurement*

Two methods of conditional sampling were employed in the present measurements. The arrangement of the hot wires for these measurements is sketched in figure 1. The filtered fluctuating streamwise velocity u_w at the edge of the sublayer was used for detection for both methods. If the signal u_w satisfied certain conditions, then one sample of Reynolds stress was found. A digital computer program was used to compare the velocity u_w with a desired constant level and the slope of u_w was also determined when the constant level was reached. The sampled uv data were treated in the following two ways.

(i) The sampled uv time segments (zero time referred to the time of detection corrected for the time lag $\Delta\tau$ of the third-order Butterworth filter;

$$\Delta\tau U_\infty/\delta^* = 1\cdot645)$$

were stored and averaged to give the average value of the samples. This is the same method as that used by Willmarth & Lu (1971) except that a correction for filter time lag was not made in that paper. The signals u, v and uv were obtained using

$$u = (u_{1n} + u_{2n})/\sqrt{2}, \quad v = (u_{1n} - u_{2n})/\sqrt{2} \tag{1}$$

and

$$uv = \tfrac{1}{2}(u_{1n}^2 - u_{2n}^2). \tag{2}$$

† The filter was a third-order Butterworth low-pass filter with half-power point at 80 Hz. It is fully described and analysed in Lu & Willmarth (1972).
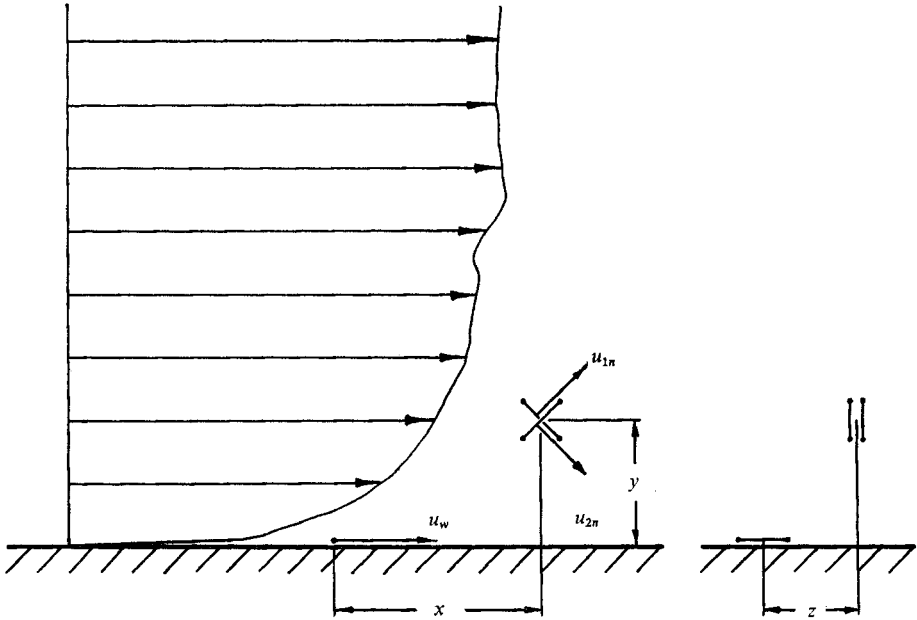
FIGURE 1. Sketch of arrangement of hot wires for measurements of u_w, u_{1n} and u_{2n}.

Let $\langle uv \rangle$ denote the average value of the samples, then,

$$\langle uv \rangle = \frac{1}{N} \sum_{i=1}^{N} (uv)_i, \tag{3}$$

where N is the number of stored samples.

(ii) The sampled uv time segment was sorted into four parts depending on which quadrant in the u, v plane the uv signal at any instant belonged to. To make the method clearer, define $h_i(\tau)$ by

$$h_i(\tau) \equiv \begin{cases} 1 & \text{for any time } \tau \text{ that the point } (u,v) \text{ is in the } i\text{th} \\ & \text{quadrant in the } u, v \text{ plane,} \\ 0 & \text{otherwise,} \end{cases} \tag{4}$$

for $i = 1, 2, 3, 4$. Next, define the four segments $uv_i(\tau)$ by

$$uv_i(\tau) \equiv h_i(\tau)\, uv(\tau). \tag{5}$$

Then, the average values of the sampled segments are

$$\langle uv_i \rangle = \frac{1}{N} \sum_{j=1}^{N} [uv_i(\tau)]_j, \tag{6}$$

where N is the number of samples. Note that the first method is related to the second method through

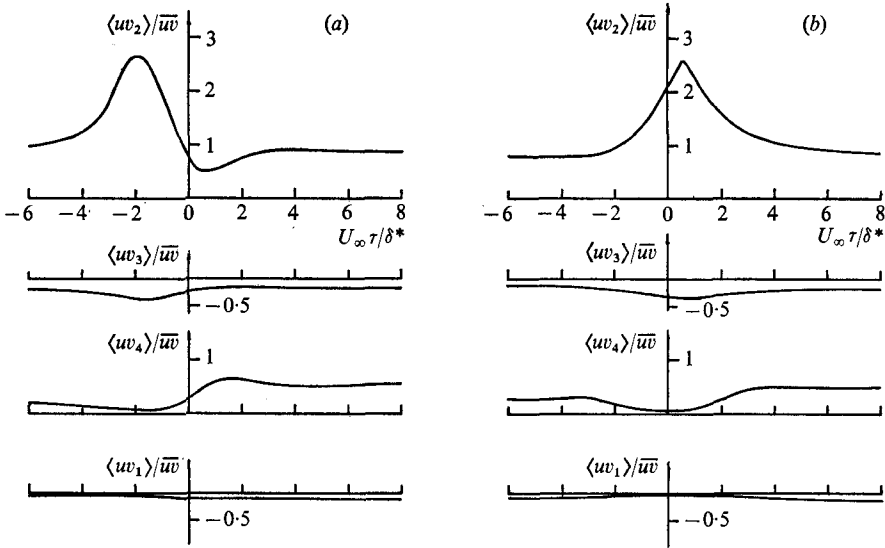$$\langle uv \rangle = \sum_{i=1}^{4} \langle uv_i \rangle. \tag{7}$$

FIGURE 2. Measurements of samples sorted Reynolds stress. $u_w/u_w' = -1$; $x/\delta^* = 0$, $y/\delta^* = 0.118$, $z/\delta^* = 0$. (a) Positive slope. (b) Negative slope.

$\langle uv_2 \rangle$ comes from the second quadrant in the u, v plane and is associated with the outflow of low-speed fluid, while $\langle uv_4 \rangle$ comes from the fourth quadrant and is associated with the inflow of high-speed fluid. $\langle uv_1 \rangle$ and $\langle uv_3 \rangle$ are the other interactions.

3.2. *Discussion of detection criteria and results of measurements*

Extensive measurements at low speed (20 ft/s) were made using these methods. Figures 2 and 3 show representative results for the non-dimensional quantities $\langle uv_i \rangle / \overline{uv}$ as functions of the non-dimensional time $U_\infty \tau / \delta^*$ with different sampling conditions (capital letters indicate the mean velocity component). The u_w wire was located at $y = 0.037$ in. from the wall, or $y^+ = 16.2$. This location was chosen on the basis of the observation by Corino & Brodkey (1969) that the approximate centre of the low-speed region near the wall was at $y^+ \approx 15$. The u_w signal was passed through a low-pass filter; see footnote above. The sampling conditions for figures 2 and 3 were that the filtered u_w signal was equal to the trigger level of $\pm u_w'$ with positive or negative slope at the trigger level. The location of the X-wire was directly above the point where u_w was measured. The centre of the X-wire was at $y = 0.07$ in., or $y^+ = 30.5$.

It is seen from figures 2(a) and (b) that there are peaks in $\langle uv_2 \rangle / \overline{uv}$ plots and valleys in $\langle uv_4 \rangle / \overline{uv}$ plots. At the time when the peak in $\langle uv_2 \rangle$ occurs, there are only small contributions to $\langle uv \rangle$ from other $\langle uv_i \rangle$. Thus, there is a large contribution to $\overline{uv}$ from bursting events when u_w is low. However, the locations of peaks in these two plots are different. For the case $u_w/u_w' = -1$ with the slope of u_w positive (the low-speed fluid being accelerated), the peak occurs before the sampling conditions are detected. For the other case ($u_w/u_w' = -1$ with negative u_w slope, i.e. the fluid speed is low and decreasing), the peak occurs after the detection. This is in agreement with the visual studies by Kim *et al.* (1968, 1971)
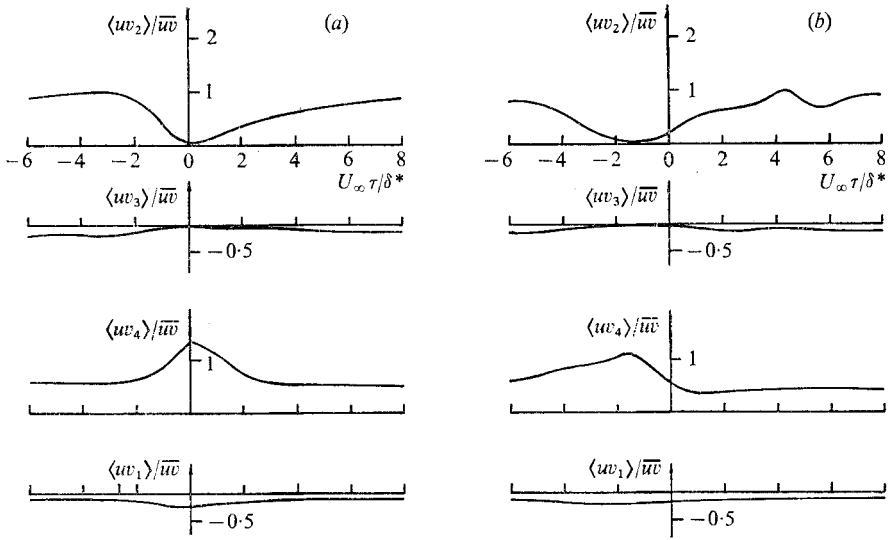
FIGURE 3. Measurements of sampled sorted Reynolds stress. $u_w/u_w' = +1$; $x/\delta^* = 0$, $y/\delta^* = 0.118$, $z/\delta^* = 0$. (a) Positive slope. (b) Negative slope.

and Corino & Brodkey (1969) that the flow speed near the wall was low before and during bursting and the velocity profile was inflexional. This result also clarifies the findings of Willmarth & Lu (1971), who measured $\langle uv \rangle/\overline{uv}$ only. Thus, these plots show that the burst occurs when the velocity at the edge of the sublayer becomes low and decreasing.

Figures 3 (a) and (b) were obtained with the trigger level set at $+u_w'$, the slope of u_w being positive and negative respectively. Peaks are seen in the $\langle uv_4 \rangle/\overline{uv}$ plots while there are valleys in $\langle uv_2 \rangle/\overline{uv}$ plots. At the time when the peak in $\langle uv_4 \rangle$ occurs, there are only small contributions to $\langle uv \rangle$ from the other $\langle uv_i \rangle$. Also the peak in the $\langle uv_4 \rangle/\overline{uv}$ plot occurs earlier when u_w is of negative slope. The peak occurs at the same time as the u_w signal reaches $+u_w'$ with positive slope. Since $\langle uv_4 \rangle$ is associated with sweeps, this finding provides additional information about the acceleration phase as observed in the visual study of Corino & Brodkey (1969). Thus, the sweep occurs when the velocity at the edge of the sublayer becomes high and increasing.

The contributions to $\langle uv \rangle$ from the sweeps are smaller than from the bursts as can be seen by comparing the magnitude of the peaks in figures 2 (b) and 3 (a). The peak observed in the $\langle uv_2 \rangle/\overline{uv}$ plot for the burst, figure 2 (b), is 2·6 times the average Reynolds stress while the peak observed in the $\langle uv_4 \rangle$ plot of figure 3 (a) associated with sweeps is 1·35 times the mean Reynolds stress. The ratio is 1·92. As the time lag becomes large, or at a time remote from the detection time, each $\langle uv_i \rangle$ approaches a constant value. As τ becomes large,

$$\langle uv_2 \rangle/\overline{uv} \to 0.85, \quad \langle uv_4 \rangle/\overline{uv} \to 0.5$$

and $\langle uv_1 \rangle/\overline{uv}$ and $\langle uv_3 \rangle/\overline{uv}$ have small negative values. The inequality of the two values for $\langle uv_2 \rangle/\overline{uv}$ and $\langle uv_4 \rangle/\overline{uv}$ is striking. The ratio of the contributions to $\overline{uv}$

from $\langle uv_2 \rangle$ and from $\langle uv_4 \rangle$ at large τ is 1·7 to 1. The contributions to $\overline{uv}$ from the bursts are considerably larger than from the sweeps. This important fact will be further studied later when the statistical properties of the uv signal are surveyed.

Similar results were obtained when the X-wire probe was placed at various stations directly downstream of the u_w wire. At each station two sets of $\langle uv_i \rangle$ were obtained using two different sampling conditions: (i) with the trigger level at $-u'_w$ and the slope of u_w negative at the trigger level and (ii) with the trigger level at $+u'_w$ and the slope of u_w positive at the trigger level. For case (i) peaks exist in $\langle uv_2 \rangle / \overline{uv}$ plots and valleys in $\langle uv_4 \rangle / \overline{uv}$ plots. At the time when the peak in $\langle uv_2 \rangle$ occurs, there are only smaller contributions to $\langle uv \rangle$ from the other $\langle uv_i \rangle$. For case (ii) peaks exist in $\langle uv_4 \rangle / \overline{uv}$ plots and valleys in $\langle uv_2 \rangle / \overline{uv}$ plots. At the time when the peak in $\langle uv_4 \rangle$ occurs, there are only smaller contributions to $\langle uv \rangle$ from the other $\langle uv_i \rangle$. Regardless of the location of the X-wire probe relative to the u_w wire, it is generally observed that the contributions to $\langle uv \rangle$ from the sweeps (case (ii)) are smaller than those from the bursts (case (i)).

At a time remote from the detection time for both cases, the product uv will not correlate with the sampling criteria. The quantity u measured at the X-wire station after this large time lag will be unrelated to the detection criterion. However, to ensure a negative value of the mean Reynolds stress, the product uv must occur at a point in the second or fourth quadrants of the u, v plane more often or with larger absolute value than in the other quadrants. Thus, the absolute values of $\langle uv_2 \rangle + \langle uv_4 \rangle$ will be larger than that of $\langle uv_1 \rangle + \langle uv_3 \rangle$. This was observed in the above measurements for both case (i) and case (ii).

Consider now a time close to the detection time and with the X-wire probe not too remote from the detection wire. In case (i) the fluid is being retarded at the detection and measuring stations. The turbulent streamwise velocity u measured at the X-wire station will most likely be less than zero. The product uv will then come from a point in the half-plane $u < 0$ of the u, v plane most of the time. Thus, larger absolute values of $\langle uv_2 \rangle$ and $\langle uv_3 \rangle$, and smaller absolute values of $\langle uv_1 \rangle$ and $\langle uv_4 \rangle$, will be observed than at times remote from the detection time. This argument explains the presence of peaks and valleys in the plots of the sampled and sorted Reynolds stress for case (i). Ensuring a negative mean Reynolds stress requires that at times close to the detection time the absolute peak value of $\langle uv_2 \rangle$ be larger than that of $\langle uv_3 \rangle$. This was observed in the measurements. Similar arguments can be applied to case (ii). In this case the fluid is being accelerated. Thus, the product uv will most likely come from a point in the half-plane $u > 0$ of the u, v plane. This leads to the presence of peaks and valleys in the plots of the sampled and sorted Reynolds stress. Also, the absolute peak value of the $\langle uv_4 \rangle$ will be larger than that of $\langle uv_1 \rangle$. All these facts were observed in the measurements.

The relation between $\langle uv \rangle$ and $\langle uv_i \rangle$ is given in (7). Figures 2(b) and 4(a) were obtained using the sampling conditions of case (i) with the X-wire probe at the same location. There is a large peak in the $\langle uv \rangle / \overline{uv}$ plot (figure 4(a)). This figure was obtained by adding the four $\langle uv_i \rangle / \overline{uv}$ in figure 2(b), thus $\langle uv_2 \rangle / \overline{uv}$ is the main contributor. Therefore, large contributions to $\langle uv \rangle$ occur when u_w
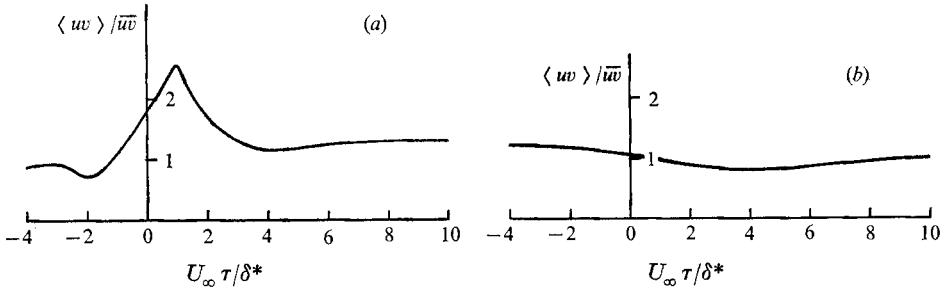
FIGURE 4. Measurements of sampled Reynolds stress. $x/\delta^* = 0$, $y/\delta^* = 0.118$, $z/\delta^* = 0$. (a) $u_w/u'_w = -1$, negative slope. (b) $u_w/u'_w = +1$, positive slope.

is low and decreasing. However, when the other case (case (ii)) is considered, the major contributor to $\langle uv \rangle$ is $\langle uv_4 \rangle/\overline{uv}$ (see figure 3(a)), but the contribution is not as large as that of $\langle uv_2 \rangle/\overline{uv}$ obtained with the sampling condition of case (i) above (see figure 2(b)). The result for case (ii) is that, in figure 4(b), there is no discernible peak in $\langle uv \rangle/\overline{uv}$. Nevertheless, almost the entire contribution to $\langle uv \rangle/\overline{uv}$, near $u_\infty \tau/\delta^* \simeq 0$, for case (ii) is caused by the sweep (note that the other three quadrants contribute nothing to $\langle uv \rangle$ at $U_\infty \tau/\delta^* \simeq 0$ for case (ii)). These results demonstrate the validity of the detection criteria, namely, that bursts or sweeps occur near the wall when the velocity near the wall is low and decreasing or high and increasing, respectively.

3.3. Spatial distribution, convection and decay of sampled Reynolds stresses $\langle uv \rangle$ and $\langle uv_i \rangle$

Consider first the burst-related events, i.e. when the sampling conditions were set at a trigger level of $-u'_w$ with the slope of u_w negative at the trigger level. The sampled sorted Reynolds stresses $\langle uv_i \rangle/\overline{uv}$ were measured with the X-wire probe at four positions directly downstream of the u_w wire at a distance of approximately $y = 0.15\delta^*$, or $y^+ \simeq 39$, from the wall. Figure 5 shows the results of the measurements plotted in a space–time format. As can be seen in this figure there is a time lag required for the occurrence of the peak in $\langle uv_2 \rangle/\overline{uv}$ plot. The origin of each plot in this figure is located vertically in proportion to the distance x of the X-wire probe from the u_w wire. Thus, the dashed line in the figure represents the space–time trajectory of the convected bursts. From the slope of this line the burst convection speed U_{CB} at this distance from the wall was found to be about 8.5 ft/s, which is somewhat less than the local mean flow velocity ($U_{CB}/U \approx 0.8$ and $U_{CB}/U_\infty \approx 0.425$) at $y = 0.15\delta^*$.

Measurements of sampled but unsorted values of $\langle uv \rangle$ at greater distances from the wall (both downstream and to the side of the u_w wire) show that the magnitude of the peak in the $\langle uv \rangle/\overline{uv}$ plot decreases as one travels outwards from the wall and spanwise at a fixed downstream station from the u_w wire. The decrease in magnitude of the peak is also observed as one travels downstream at a fixed distance from the wall. From these more extensive measurements of $\langle uv \rangle/\overline{uv}$ (see Lu & Willmarth 1972), it is apparent that the bursts are confined to a narrow
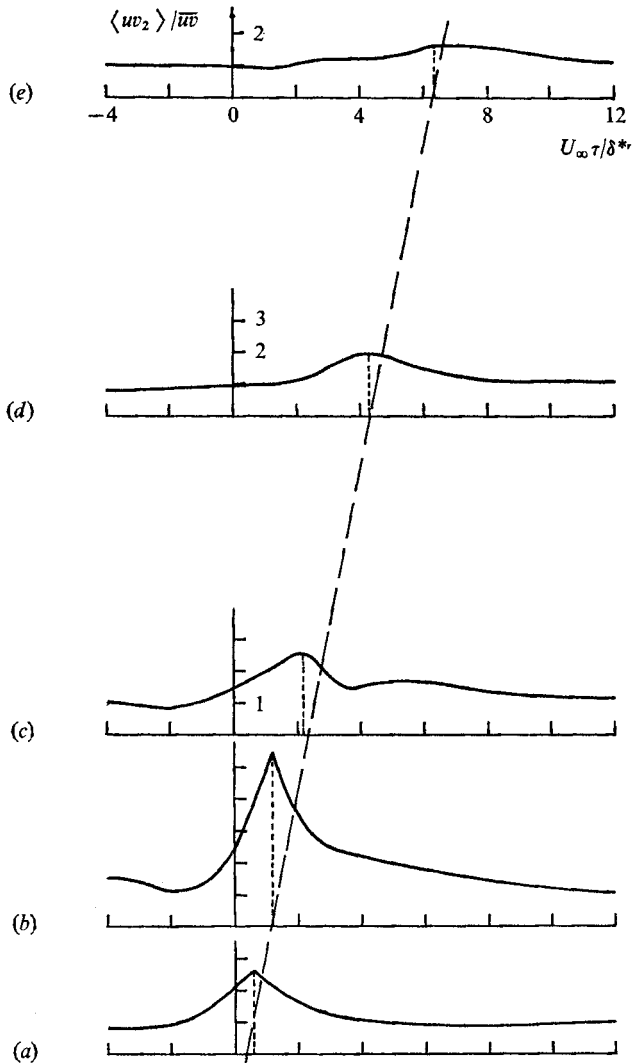
FIGURE 5. Convection and decay of sampled sorted Reynolds stress $\langle uv_2 \rangle / \overline{uv}$, with sampling conditions $u_w/u'_w = -1$, negative slope; $y/\delta^* \approx 0.169$, $z/\delta^* = 0$ and $U_\infty \simeq 20$ ft/s. (a) $x/\delta^* = 0$, (b) $x/\delta^* = 0.34$, (c) $x/\delta^* = 0.84$, (d) $x/\delta^* = 1.69$, (e) $x/\delta^* = 2.53$.

region in the spanwise direction near the wall and downstream from the u_w wire. However, the region of disturbance in the direction normal to the wall increases from a size $y/\delta^* = 0.506$ at $x/\delta^* = 0$ to a size $y/\delta^* = 0.912$ at $x/\delta^* = 1.686$ and increases even more as one travels further downstream. There is still some coherent contribution to the sampled value $\langle uv_2 \rangle$ even at a station $x/\delta^* = 2.53$ downstream of the u_w wire but near the wall. The data from which these conclusions were drawn are too numerous to include here; see Lu & Willmarth (1972).

At a fixed station downstream of the u_w wire ($z = 0$, x fixed, y variable), **one** finds that, at a certain distance from the wall, the peak in the $\langle uv \rangle / \overline{uv}$ curve will occur without a time delay. This distance from the wall increases as one
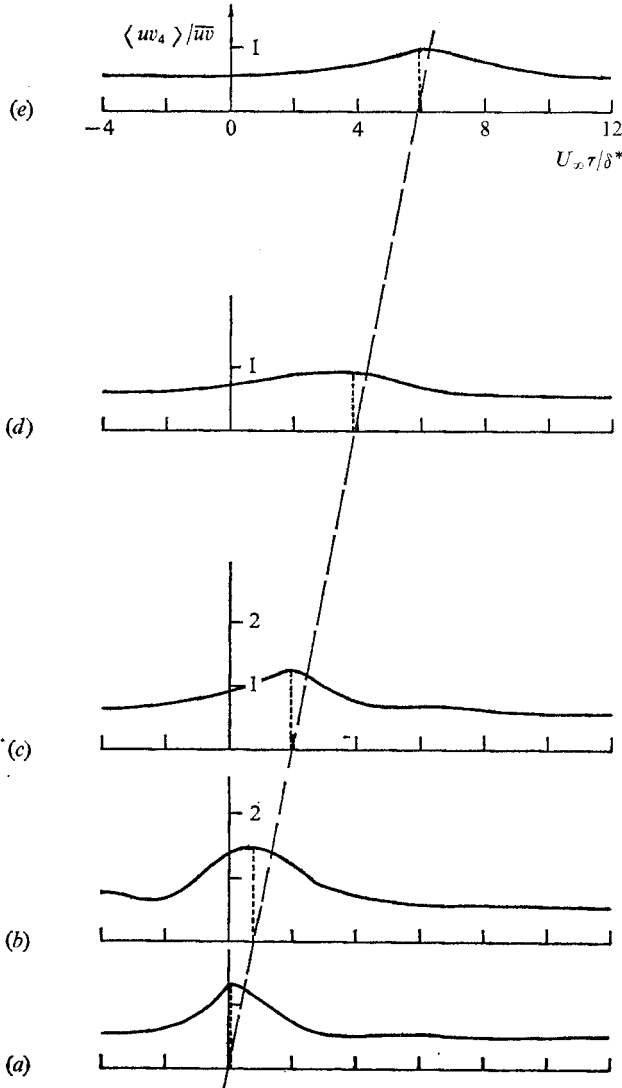
FIGURE 6. Convection and decay of sampled sorted Reynolds stress $\langle uv_4 \rangle/\overline{uv}$, with sampling conditions $u_w/u'_w = +1$, positive slope; $y/\delta^* \approx 0.169$, $z/\delta^* = 0$ and $U_\infty \simeq 20\,\mathrm{ft/s}$; (a)–(e) same as in figure 5.

moves downstream. The line in the x, y plane on which the peaks occur without a time delay travels outwards from the surface at an angle of $16°$–$20°$. The fact that the line of maximum $\langle uv \rangle/\overline{uv}$ is inclined downstream does not mean that this indicates the shape of the line of maximum $\langle uv \rangle$ in the flow pattern of a typical burst. It simply means that on average the enlarging and convectively sheared bursting flow patterns produce this result when averages over many randomly occurring (in space and time) bursting flow patterns are observed by a single X-wire. Indeed, some bursts that are detected near the wall may be so young that they do not reach the X-wire when it is far from the wall. Thus, for larger distances from the wall, the sampled X-wire signal is produced by the older, more

lasting features of the turbulent bursts (i.e. there is a spatial filtering effect which one must consider).

Consider now the sweep-related events, i.e. when the sampling conditions were set at trigger level of $+u'_w$ and with the slope of u_w positive at the trigger level. The sampled sorted Reynolds stresses $\langle uv_4\rangle/\overline{uv}$ from sweeps are displayed in figure 6 in the same format as was used for figure 5 and at the same distances downstream and from the wall. No measurements of sampled Reynolds stress $\langle uv\rangle/\overline{uv}$ were made since there would be no peak in the $\langle uv\rangle/\overline{uv}$ plot as was noted in the last section. The behaviour of the magnitude of the peak in $\langle uv_4\rangle/\overline{uv}$ is similar to that for the bursts. It decreases as one travels outwards from the wall or downstream at a fixed distance from the wall. The speed of convection of the sweeps is represented by the dashed line in figure 6. The sweep convection speed U_{CS} was found to be nearly the same as the burst convection speed. Thus, $U_{CS}/U \simeq U_{CB}/U \simeq 0\cdot8$ and $U_{CB}/U_\infty \simeq U_{CS}/U_\infty \simeq 0\cdot425$.

Rough estimates of the speed of convection of the bursts were also made at various larger distances from the wall. The burst convection speed U_{CB} was found to increase with distance from the wall, however we have not been able to obtain accurate measurements of convection speed at greater distances from the wall. It appears from other measurements (Willmarth & Wooldridge 1962) that wall pressure disturbances, for example, are convected at speeds ranging from $0\cdot58 < U_C/U_\infty < 0\cdot83$. The lower convection speeds are associated with small-scale eddies near the wall. The present measurements therefore suggest that the small-scale burst pattern emanates from the wall region, travels outward and grows larger as it is carried downstream. As it enlarges it also is sheared and distorted because the convection velocity is higher further from the wall. The evolving and enlarging burst pattern soon loses coherence with the detector criterion near the wall ($u_w = -u'_w$ with negative slope), so that the sampled values of $\langle uv_2\rangle$ can no longer reveal the burst structure. The bursts still exist, however, as will become apparent in §4.4.

Before the detector criterion fails, the peak in the $\langle uv\rangle/\overline{uv}$ value which represents the region of disturbance caused by the burst increases from a size $y/\delta^* = 0\cdot506$ at $x/\delta^* = 0$ to a size of $y/\delta^* = 0\cdot912$ at $x/\delta^* = 1\cdot686$ and increases even more as one travels further downstream. There is still some contribution to $\overline{uv}$ even at a station at $x/\delta^* = 2\cdot53$ downstream of the u_w detector wire. The spanwise extent of the region of disturbance is confined to a narrow swept-back region with an included angle of approximately 20° centred upon the free-stream direction.

4. Statistical properties of the uv signal in the turbulent boundary layer

The use of a digital computer for data reduction facilitates the rapid investigation of various statistical properties of large samples of the random signal uv. In this section we first establish a connexion with past results from measurements of the Reynolds stress distribution $-\rho\,\overline{uv}$ throughout the boundary layer. Next the probability distribution of uv and the contributions of bursts and sweeps to $\overline{uv}$ from various portions of the boundary layer are studied.
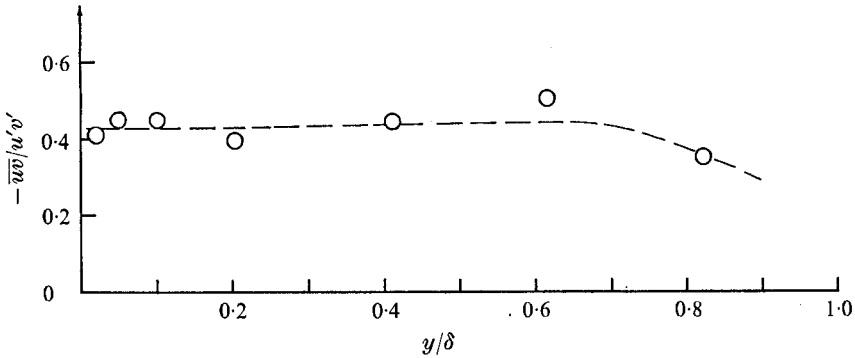
FIGURE 7. Measurements of correlation coefficients in a turbulent boundary layer; $U_\infty \approx 20\,\text{ft/s}$.

4.1. Correlation coefficient distribution

The correlation coefficient $\overline{uv}/u'v'$ is shown in figure 7 as a function of y/δ. It is nearly constant throughout the boundary layer and assumes a mean value of $-0\cdot44$. Some previous results are discussed here for comparison. Townsend (1951) reported a value of $-0\cdot48$ for most of the turbulent boundary layer. Klebanoff (1954) gave a value of $-0\cdot5$ while Laufer (1953) showed a value of $-0\cdot45$ for $y^+ > 15$ in a pipe flow. Tritton (1967) reported a value of $-0\cdot46$. A value of $-0\cdot5$ was given by Kim et al. (1968) for $y^+ < 100$. In the greater part of the channel flows the correlation coefficient was $-0\cdot4$ to $-0\cdot5$ as reported by Reichardt (1938), Eckelmann (1970) and Wallace et al. (1972). Even at a location very close to the wall a value of $-0\cdot45$ is approached as was shown by Coantic (1965), who used the Navier–Stokes equation with a power-series expansion of each turbulent variable in the neighbourhood of the wall to give an expression for the correlation coefficient in terms of measured quantities. Thus, a value of $-0\cdot45$ for the correlation coefficient can be assumed for most of the turbulent boundary layer even very close to the wall. This agrees with the present measurements.

4.2. Probability density distributions

The probability density distributions β_u and β_v of u and v are shown in figure 8, and were measured at a distance of $0\cdot07\,\text{in.}$ from the wall, or $y^+ = 30\cdot5$. The Gaussian distribution is also shown for reference. The turbulent velocity u is seen to follow the normal Gaussian distribution somewhat more closely than v. The deviations from the normal Gaussian distribution consist of a rather high value of $0\cdot5$ for β_v reached at $v = 0$ as compared with a value of $0\cdot4$ for the normal Gaussian distribution. Also, the β_u curve is slightly skewed to the negative side of u/u' and the β_v curve to the positive side of v/v'.†

The probability density distributions β_{uv} of uv fluctuations were measured at various distances from the wall. The results were found to be very similar to

† Zaric (1972) has recently reported interesting measurements of β_u near the wall and in the sublayer which show rather large deviations from a Gaussian distribution. We were not able to conduct measurements of uv in this interesting region close to the wall owing to the difficulty of constructing small X-wire probes.
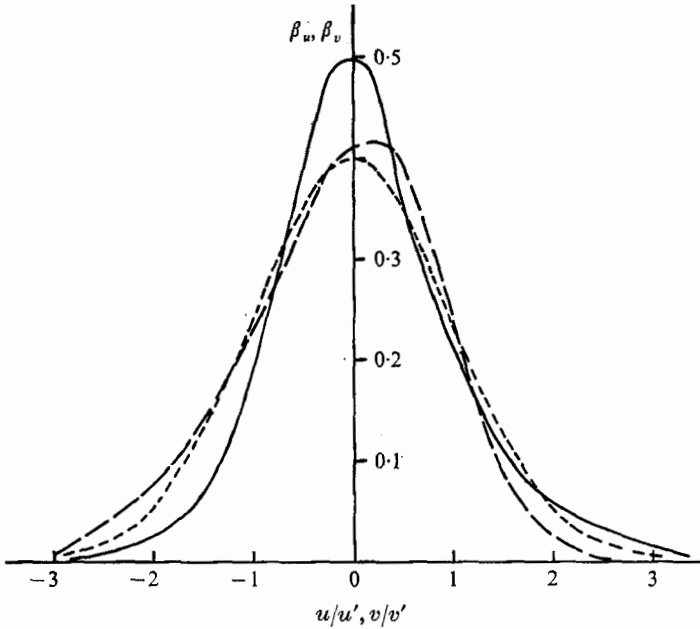
FIGURE 8. Probability density distributions of u and v measured at a distance $y^+ = 30.5$ from the wall in a turbulent boundary layer; $U_\infty \approx 20\,\text{ft/s}$. $---$, β_u; ———, β_v; $----$, Gaussian.
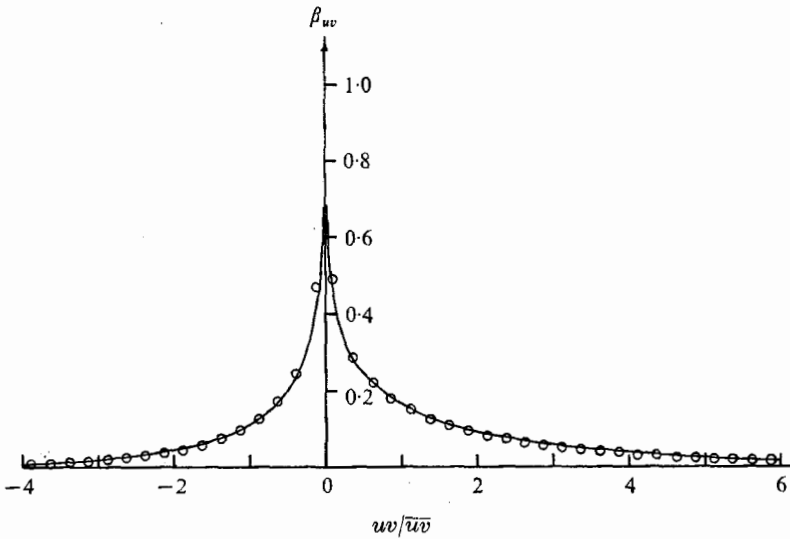
FIGURE 9. Probability density distribution of the uv signal; $y/\delta^* = 0.91$, $U_\infty \simeq 20\,\text{ft/s}$. $\bigcirc$, measurement; ———, equation (9).

that reported by Willmarth & Lu (1971) at $y^+ \approx 30$. This distribution has long tails for extreme values of uv and a sharp peak at $uv = 0$. A typical distribution is shown in figure 9, and was measured at a distance of 0.54 in. from the wall, or $y/\delta^* = 0.912$. Also, Gupta & Kaplan (1972) report measurements of β_{uv} very near the wall which are in reasonable agreement with ours at $y^+ \approx 30$, except that their maximum value of β_u does not occur at $uv = 0$.

The oddly shaped probability density distribution of the uv signal is not surprising if one assumes that u and v are two statistically dependent random variables with correlation coefficient $R = -0.44$, each obeying the Gaussian distribution law. The joint-probability-density distribution function of the product uv is

$$P(u_1, u_2) = \frac{1}{2(1-R^2)^{\frac{1}{2}}} \exp \left\{ \frac{-1}{2(1-R^2)} (u_1^2 - 2Ru_1u_2 + u_2^2) \right\}, \tag{8}$$

where $\quad u_1 = u/u_1, \quad u_2 = v/v' \quad$ and $\quad R = \overline{u_1 u_2} = \overline{uv}/u'v' = -0.44.$

After some transformations and integrations, see Lu & Willmarth (1972) for details, the probability density distribution of the normalized $uv/\overline{uv}$ signal can be found from (8). The result is

$$\beta_{uv}(uv/\overline{uv}) = \frac{1}{\pi} \frac{|R|}{(1-R^2)^{\frac{1}{2}}} \exp \left(\frac{R^2 uv/\overline{uv}}{1-R^2} \right) K_0 \left(\left| \frac{Ruv/\overline{uv}}{1-R^2} \right| \right), \tag{9}$$

where K_0 is the zeroth-order K Bessel function. This distribution is also included in figure 8. The agreement with measurements appears to be satisfactory. Note that, as $uv \to 0$, the Bessel function approaches infinity. Thus, $\beta_{uv} \to \infty$ as $uv \to 0$. The peak at $uv = 0$ in the measured probability density distribution is thus expected. From the shape of this distribution, the intermittent character of the uv signal is expected since most of the time the uv signal will stay around $uv = 0$.

4.3. Contributions to $\overline{uv}$ from different events

To understand better the nature of contributions to $\overline{uv}$ from the different events, contributions to $\overline{uv}$ from different regions in the u, v plane were measured. The measurements were made with the X-wire at various distances from the wall. The u, v plane was divided into five regions as shown in figure 10. In the figure, the cross-hatched region is called a 'hole', and is bounded by the curves $|uv| = $ constant. The four quadrants excluding the 'hole' are the other four regions. The size of the 'hole' is decided by the curves $|uv| = $ constant. Introduce the parameter H and let $|uv| = Hu'v'$, where u' and v' are the local root-mean-square values of the u and v signals. The parameter H is called the hole size. With this scheme, large contributors to $\overline{uv}$ from each quadrant can be extracted leaving the smaller fluctuating uv signal in the 'hole'. The contribution to $\overline{uv}$ from the 'hole' corresponds to the contribution during the more quiescent periods, while the second quadrant represents the burst-like events and the fourth quadrant the sweep-like events.

The contributions to $\overline{uv}$ from the four quadrants were computed from the following equations:

$$\frac{\widetilde{uv_i}(H)}{\overline{uv}} = \frac{1}{\overline{uv}} \lim_{T \to \infty} \frac{1}{T} \int_0^T uv(t) S_i(t, H) \, dt \quad (i = 1, 2, 3, 4), \tag{10}$$

where the subscript i refers to the ith quadrant and

$$S_i(t, H) = \begin{cases} 1 & \text{if } |uv(t)| > Hu'v' \text{ and the point } (u, v) \text{ in the} \\ & \quad u, v \text{ plane is in the } i\text{th quadrant,} \\ 0 & \text{otherwise.} \end{cases} \tag{10a}$$
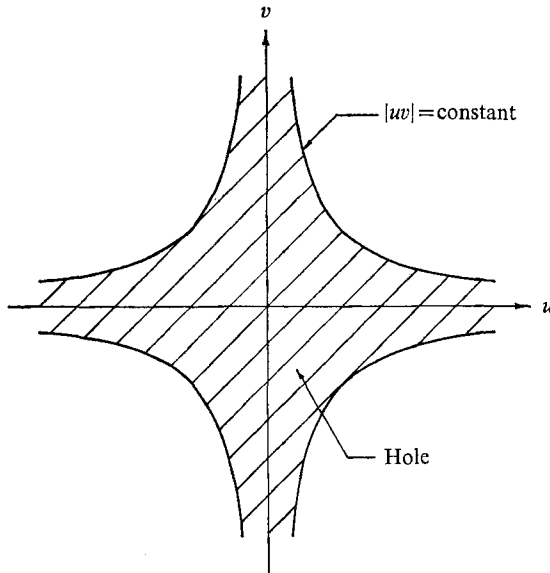
FIGURE 10. Sketch of 'hole' region in the u, v plane.

The contribution to $\overline{uv}$ from the 'hole' region was obtained from

$$\frac{\widetilde{uv}_h(H)}{\overline{uv}} = \frac{1}{\overline{uv}} \lim_{T \to \infty} \frac{1}{T} \int_0^T uv(t)\, S_h(t, H)\, dt, \tag{11}$$

where
$$S_h(t, H) = \begin{cases} 1 & \text{if } |uv(t)| \leqslant Hu'v', \\ 0 & \text{otherwise.} \end{cases} \tag{11a}$$

These five contributions $\widetilde{uv}_i$ and $\widetilde{uv}_h$ are all functions of the hole size H and

$$\sum_{i=1}^4 \frac{\widetilde{uv}_i(H)}{\overline{uv}} + \frac{\widetilde{uv}_h(H)}{\overline{uv}} = 1. \tag{12}$$

Typical results of the measurements at low speed are shown in figures 11 (*a–c*). There was only one measurement for the case of high-speed flow and this was made at a distance of $y^+ = 265$ from the wall. This result is shown in figure 12. For the low-speed measurements, the results were obtained with the X-wire at various distances from the wall. The results were very similar for both high and low Reynolds numbers regardless of the X-wire probe location in the turbulent boundary layer. In these figures, curves representing the fraction of the total time that uv signal spent in the 'hole' region are also included. As can be seen, for a large portion of the time, $|uv|$ is very small. This is expected from the probability density distribution of the uv signal. It can also be observed from an actual trace of the uv signal that, for a large fraction of time, the uv signal is approximately zero. This fact is also shown by the contribution curve related to the 'hole', in which the contribution remains small in spite of large time of occupancy. As a matter of fact, these two curves, i.e. the fraction of the total time in the 'hole' and the contribution to $\overline{uv}$ from the 'hole' region, can be
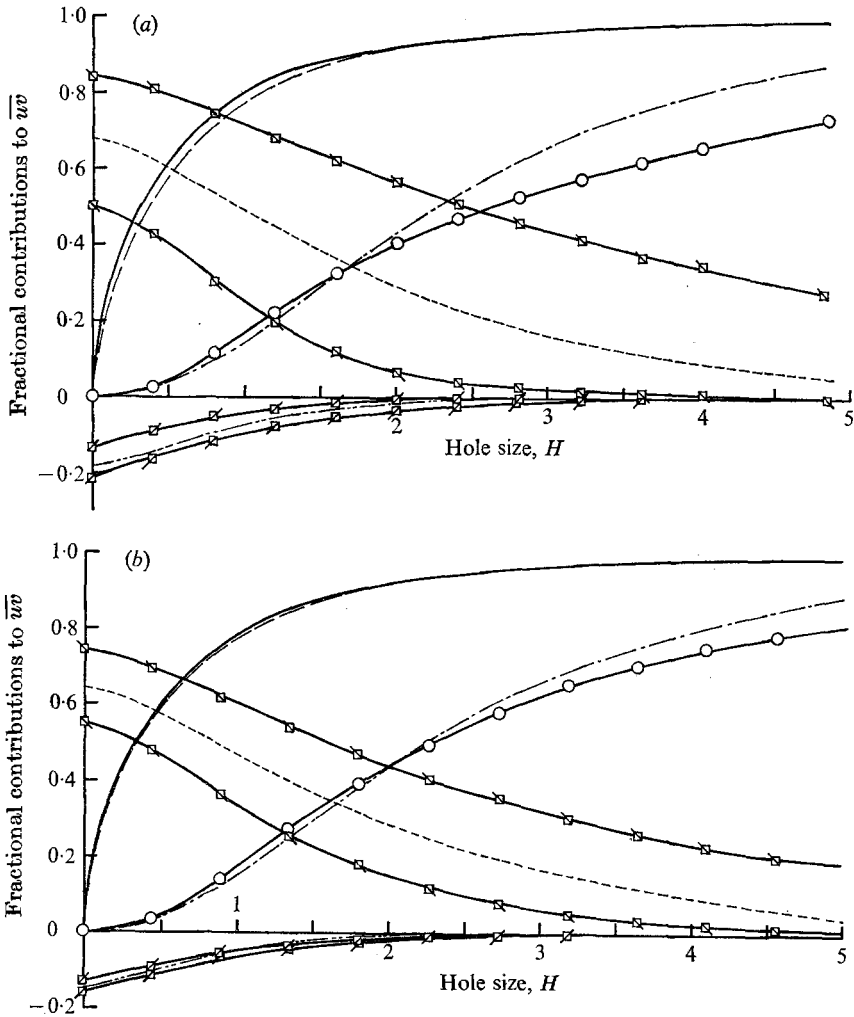
FIGURES 11 (a, b). For legend see p. 497.

derived from the assumption of joint-normality of u and v signals using (9); for details see Lu & Willmarth (1972). The predicted curves are included in figures 11 and 12 for comparison. The agreement between measurements and predictions is very good except at the point very close to the wall and in the outer intermittent region.

The assumption of joint-normality of u and v signals also implies that the contribution $\widetilde{uv_2}$ to $\overline{uv}$ from the second quadrant should equal that from the fourth quadrant, $\widetilde{uv_4}$. Similarly, $\widetilde{uv_1} = \widetilde{uv_3}$. The predicted curves for $\widetilde{uv_2}$ and $\widetilde{uv_1}$ are also shown on the figures. The deviation from joint-normality is apparent, since $\widetilde{uv_2} \neq \widetilde{uv_4}$ and $\widetilde{uv_1} \neq \widetilde{uv_3}$, regardless of the flow speed and the location in the turbulent boundary layer. As can be seen, the largest contribution comes from the second quadrant and is burst-like. The second largest contribution is $\widetilde{uv_4}$ and is sweep-like. The contributions from $\widetilde{uv_1}$ and $\widetilde{uv_3}$ are negative and relatively
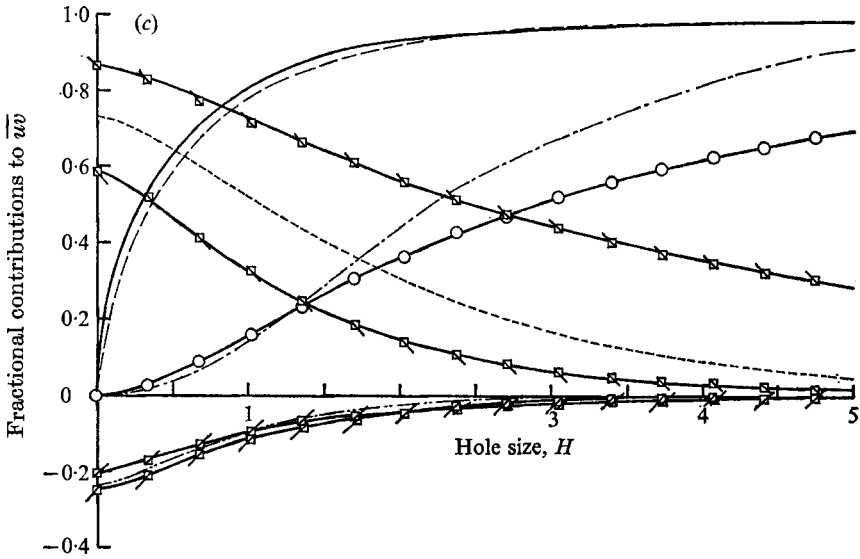
FIGURE 11. Measurements of the contributions to $\overline{uv}$ from different events at various distances from the wall. $\widetilde{uv}_1/\overline{uv}$: ⧄, measured; —··—, computed. $\widetilde{uv}_2/\overline{uv}$: ◹, measured; ----, computed. $\widetilde{uv}_3/\overline{uv}$: ⧄, measured; ——, computed. $\widetilde{uv}_4/\overline{uv}$: ◹, measured; ----, computed. $\widetilde{uv}/\overline{uv}$: ○, measured; ———, computed. Fraction of time in 'hole': ———, measured; ———, computed. $U_\infty \simeq 20\,\text{ft/s}$, $Re_\theta \simeq 4\cdot230$. (a) $y/\delta = 0\cdot021$. (b) $y/\delta = 0\cdot052$. (c) $y/\delta = 0\cdot823$.
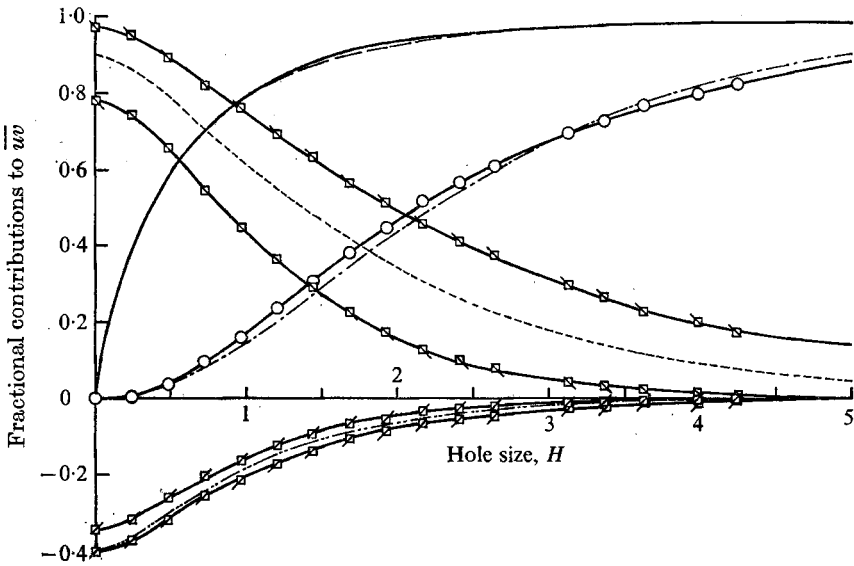
FIGURE 12. Measurements of the contributions to $\overline{uv}$ from different events. $U_\infty \simeq 200\,\text{ft/s}$, $Re_\theta \simeq 38\,000$, $y/\delta \simeq 0\cdot014$ ($y^+ \simeq 265$). Notation as in figure 11.
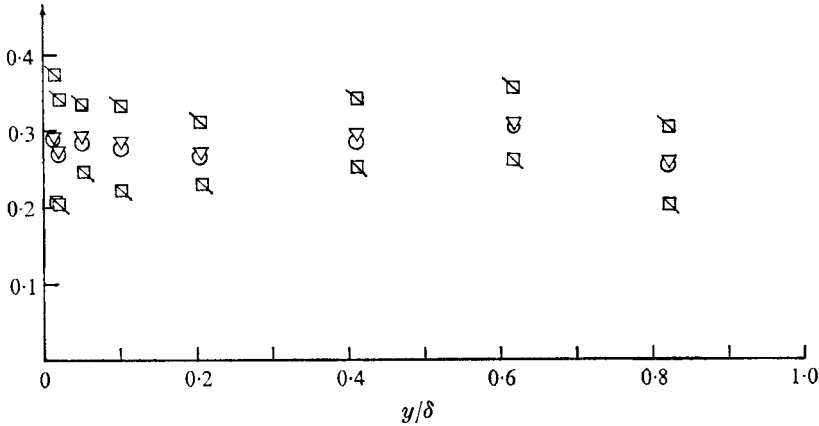
FIGURE 13. Distributions of $\widetilde{uv_2}/u'v'$ and $\widetilde{uv_4}/u'v'$ with $H = 0$, $Re_\theta \simeq 4230$. $\boxtimes$, $-\widetilde{uv_2}/u'v'$; $\boxtimes$, $-\widetilde{uv_4}/u'v'$; ∇, $-(\widetilde{uv_2}+\widetilde{uv_4})/2u'v'$; $\bigcirc$, $-(\widetilde{uv_2}+\widetilde{uv_4})/2u'v'$, computed.

small. When the hole size H becomes large, there are only two contributions. One is $\widetilde{uv_2}$ and the other one comes from the 'hole' region. Thus the importance of the burst-like events in the turbulent boundary layer is obvious. At a hole size of $H = 4\cdot5$, which amounts to $|uv| > 10|\overline{uv}|$, there is still a 15–30 % contribution to $\overline{uv}$ from the second quadrant, i.e. $\widetilde{uv_2}/\overline{uv} \approx 0\cdot15$–$0\cdot30$. At this level there are almost no contributions from the other three quadrants.

4.4. *Results for the burst-like and sweep-like events*

Results will be discussed here regarding the contributions to $\overline{uv}$ from burst- and sweep-like events. Figure 13 shows the distribution of $\widetilde{uv_2}/u'v'$, $\widetilde{uv_4}/u'v'$, their average values and the predicted average values, with $H = 0$ across the boundary layer. It is understood that the hole size is set at zero ($H = 0$) in this section. Both $\widetilde{uv_2}/\overline{uv}$ and $\widetilde{uv_4}/\overline{uv}$ are nearly constant in the boundary layer except very close to the wall and near the edge of the boundary layer. It is found that $\widetilde{uv_2}/u'v' \approx -0\cdot34$ and $\widetilde{uv_4}/u'v' \approx -0\cdot24$, or $\widetilde{uv_2}/\overline{uv} \approx 0\cdot77$ and $\widetilde{uv_4}/\overline{uv} \approx 0\cdot55$. Thus, burst-like events account for 77 % of the local Reynolds stress and the sweep-like events for 55 %. This leaves -32 % of local Reynolds stress to the other two negative contributors. As can be seen from figure 13, the average of the values of $\widetilde{uv_2}/u'v'$ and $\widetilde{uv_4}/u'v'$ predicted from the assumption of the joint-normality of u and v are in satisfactory agreement with the measured values. It should be pointed out here that, even though the u and v signals are not jointly normal as noted in this study and the u and v signals are not Gaussian as noted before, in § 4.2, the assumption of joint-normality of u and v leads to a reasonably good prediction for quantities such as the fraction of time spent in hole, the fractional contribution to $\overline{uv}$ from hole, the probability density distribution of the uv signal and average value $(\widetilde{uv_2}+\widetilde{uv_4})/(2u'v')$.

The ratio of the contribution to $\overline{uv}$ from the burst-like events and that from the sweep-like events is plotted in figure 14 as a function of y/δ. There is a sharp rise near the wall while for most of the boundary layer the ratio is nearly constant
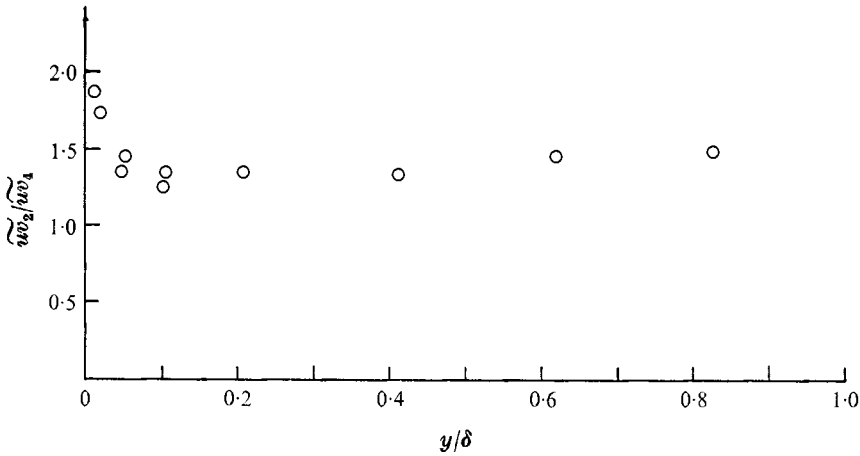
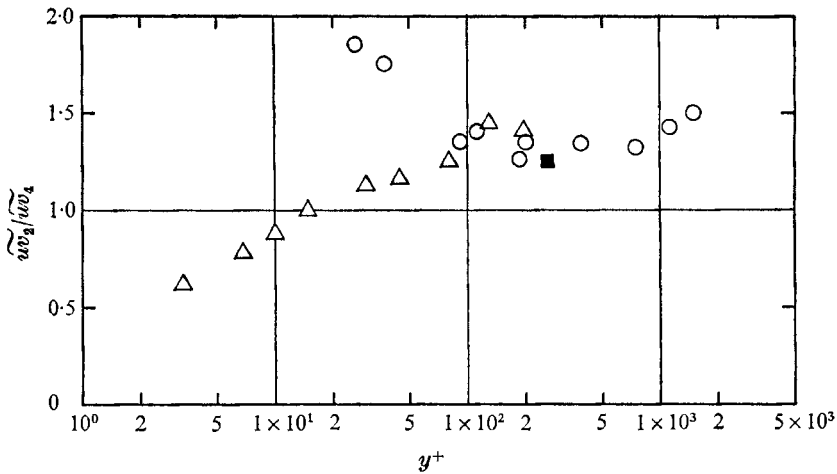FIGURE 14. Distribution of the ratio $\widetilde{uv_2}/\widetilde{uv_4}$ with $H = 0$, $Re_\theta \simeq 4230$.

FIGURE 15. The ratio $\widetilde{uv_2}/\widetilde{uv_4}$ with $H = 0$ as a function of y^+. $\bigcirc$, $Re_\theta \simeq 4230$; $\blacksquare$, $Re_\theta \simeq 38\,000$; $\triangle$, channel flow, Wallace *et al.* (1972), Re_θ very low.

with a value of 1·35. The single high-speed measurement gave a value of 1·25, which was measured at $y/\delta = 0.014$ or $y^+ = 265$. The results are replotted in figure 15 as a function of y^+. In this figure, the results obtained by Wallace *et al.* (1972) at a much lower Reynolds number in a channel flow are included. It turns out that contributions to $\overline{uv}$ from the sweep period are approximately the same as those in Wallace *et al.* (1972) but that the present results show larger contributions to $\overline{uv}$ during the burst period. The reason for this disagreement may be due to the difference in Reynolds number. The results for the present measurements (figure 15) seem to scale with the wall-region variables even though the two flow conditions considered differ greatly in Reynolds number ($Re_\theta = 4230$ and $38\,000$). Although there is only one measurement for the high Reynolds number flow, it is conjectured that the Reynolds number similarity may hold. This would imply that the nature of the fluctuating turbulent structure in the wall region is similar

above $Re_\theta \simeq 4000$ but that at very low Re_θ, as in the work of Wallace *et al.* (1972), significant changes in the structure of the turbulent fluctuations occur. It is interesting to note that, at higher Reynolds numbers in the present work, the contribution to $\overline{uv}$ during the burst period is larger than that found by Wallace *et al.* (1972). However, a word of caution is in order: it is possible that significant measurement errors may be caused by operating hot wires of hot-film probes in the region very near the wall, where the level of turbulent fluctuations is very high ($u'/U \simeq 0.4$) and the mean shear $\partial U/\partial y$ is also very high. Accordingly, it remains a subject for further research to determine the reason for the difference between the present measurements and those of Wallace *et al.* (1972) near the wall.

5. Mean periods and scales of bursts and sweeps

In the visual studies of Runstadler, Kline & Reynolds (1963), Schraub & Kline (1965) and Kim *et al.* (1968, 1971), the mean time intervals $\bar{T}_B$ between bursts were measured by visual counting of the violent events of ejection near the wall in a turbulent boundary layer. Kim *et al.* found that the mean time interval $\bar{T}_B$ was nearly the same as the time lag required to obtain the second mild maximum in the curve of the autocorrelation coefficient R_{uu} of the fluctuating streamwise velocity. By a complex processing of a hot-wire signal in a turbulent boundary layer Rao *et al.* (1969, 1971) were able to measure the mean time interval between bursts. They showed, in a summary of their own and other† data obtained over a wide range of Reynolds numbers, that the mean burst period $\bar{T}_B$ scaled with outer rather than inner boundary-layer flow variables. Among their summarized data, there was only one measurement of $\bar{T}$ for high Reynolds number flow ($Re_\theta = 38000$). This was obtained from the second mild maximum in R_{uu} measured by Tu & Willmarth (1966). We have recently determined (Lu & Willmarth 1973) that the second mild maximum in R_{uu} in that data was produced by a low-pass filter used during our (1966) measurements of R_{uu}. Therefore the value of $\bar{T}$ at $Re_\theta = 38000$ that is quoted in Rao *et al.* (1971) is not valid.

In any process of counting the number of bursts a definitive identification of bursts is required. This represents difficulties both in visual studies and in hot-wire measurements. In visual studies bursts of varying magnitude are observed embedded in a background of other turbulent fluctuations. When an event is not extremely violent and/or coherent, it is up to the observer to decide whether it is a burst or not. Very much greater difficulties are present in the measurement of the mean burst period from a trace of a single hot-wire signal because only the velocity at one point in a complex bursting pattern can be observed.

In the hot-wire measurements of Rao *et al.* (1969, 1971), the signal u was passed through a band-pass filter to make 'bursts' stand out more clearly (we are not certain from their paper, whether or not the u signals were differentiated before filtering). First, as pointed out by Kim *et al.* (1971), it remains to be determined whether this process will show the phenomenon of 'oscillatory motion' in the

---

† Rao *et al.* (1971) summarized the results for the mean burst period $\bar{T}$ obtained from the papers by Kim *et al.* (1968), Schraub & Kline (1965), Runstadler *et al.* (1963) and Laufer & Badri Narayanan (1971).

second stage of the bursting process observed by Kim *et al.* (1968, 1971). Second, even if this technique does make the burst stand out, counting the number of bursts using human eyes is somewhat arbitrary since the 'bursts' are not too well organized or clearly identifiable in the traces of the processed u signal (see Rao *et al.* 1971, figure 1). However, Rao *et al.* arrived at a characteristic time, called $\overline{T}_m$, for the burst period. The procedure they followed was the following.

(a) The hot-wire signals filtered with a narrow pass band were recorded on graph paper.

(b) After central strips of various widths had been blocked out (amplitude discriminator setting), bursts were presumed to occur when the filtered signal exceeded a given discriminator level but only if the time interval after the previous burst was greater than twice the period of the centre frequency of the pass band of step (a).

(c) Mean burst rates were plotted against the amplitude discriminator settings.

(d) An optimum range of the discriminator settings over which the precise value of the setting was immaterial was found. The burst rate found in this range was the characteristic time $\overline{T}_m$.

As was pointed out by Rao *et al.* (1971) the optimum range of discriminator levels was not as wide as one might wish. It turns out that at the optimum discriminator setting the burst rate is a maximum (i.e. at high discriminator settings fewer excursions of the filtered u signal above the discriminator setting occur and for low discriminator settings the more frequent excursions above the lower setting are not counted owing to rule (b)). In procedure (b), 'the periods of activity, i.e. stretches of signal beyond this strip, were counted as separate bursts only if the time interval between them was greater than twice the basic period corresponding to the mid-frequency in the selected pass band'. This leads one to speculate what the situation will be if, instead of 'twice the basic period', some other factor times the basic period is used. The burst rate will then be a function of this factor. Then, the optimum range obtained in procedure (d) may shift to another discriminator setting depending on the value of the factor. Thus, the characteristic time $\overline{T}_m$ will not be the same.

In the present study we attempted to estimate, in a different manner, the characteristic times related to bursts and sweeps and their durations. Similar difficulties, mainly definitive identification of bursts and sweeps, were encountered. Extensive measurements were made, in a consistent manner, for the low-speed flow across the turbulent boundary layer. A single high-speed measurement was also made to study the Reynolds number effect on the burst and sweep rates.

5.1. *Measurements of burst and sweep period*

As is evident from the measurements of sampled sorted Reynolds stress, there is a large contribution to $\overline{uv}$ during the bursts. A large peak in the uv signal was observed (see the measurements of Willmarth & Lu (1971)) which came from the second quadrant of the u, v plane. Serious difficulties are encountered when it is desired to obtain definite identification of bursts from values of uv measured at a single point. Assume that, if the uv signal reaches or exceeds a certain specified
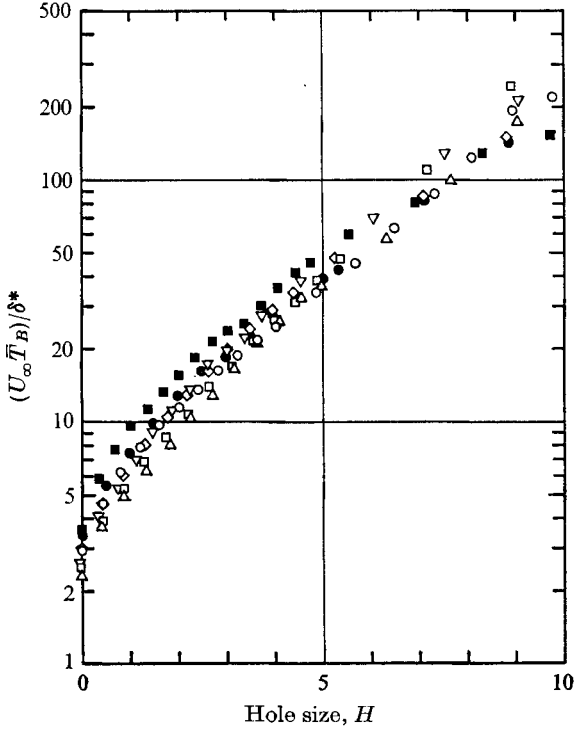
FIGURE 16. Mean time interval between bursts as a function of hole size H and distance from wall; $Re_\theta \simeq 4230$. O, $y/\delta = 0.021$; $\triangle$, $y/\delta = 0.052$; $\square$, $y/\delta = 0.103$; ∇, $y/\delta = 0.206$; $\diamondsuit$, $y/\delta = 0.412$; ●, $y/\delta = 0.618$; ■, $y/\delta = 0.823$.

level (i.e. hole size H) in the second quadrant, a burst occurs. By counting the number of times the above conditions are detected in a given time interval, the mean time interval $\overline{T}_B$ between burst contributions at a given hole size can be found. The non-dimensional mean time interval $U_\infty \overline{T}_B/\delta^*$ between bursts is shown in figure 16 as a function of the hole size H with the distance y/δ from the wall as a parameter. These data were obtained from the low-speed ($U_\infty \approx 20\,\mathrm{ft/s}$) measurements. The mean time interval between bursts exceeding a given H is nearly independent of the distance from the wall throughout the turbulent boundary layer. On the other hand, the mean time interval $\overline{T}_B$ between bursts exceeding a given value of H increases rapidly as H is increased, see figure 16. A satisfactory criterion for determining $\overline{T}_B$ should have the property that the value of $\overline{T}_B$ determined from the criterion is independent of small changes in the criterion. In figure 16, the absence of a plateau in the variation of $\overline{T}_B$ as a function of H indicates that the value of H alone is not an acceptable criterion for determining the actual value of the mean burst rate. However, upon close examination of the plots of the contributions to $\overline{uv}$ from different events at different distances from the wall (figures 11 and 12) a unique and consistent feature is observed. As the hole size becomes large, the contributions to $\overline{uv}$ from quadrants one, three and four vanish more rapidly than contributions from the second quadrant. It is observed that, when H reaches a value of between 4 and
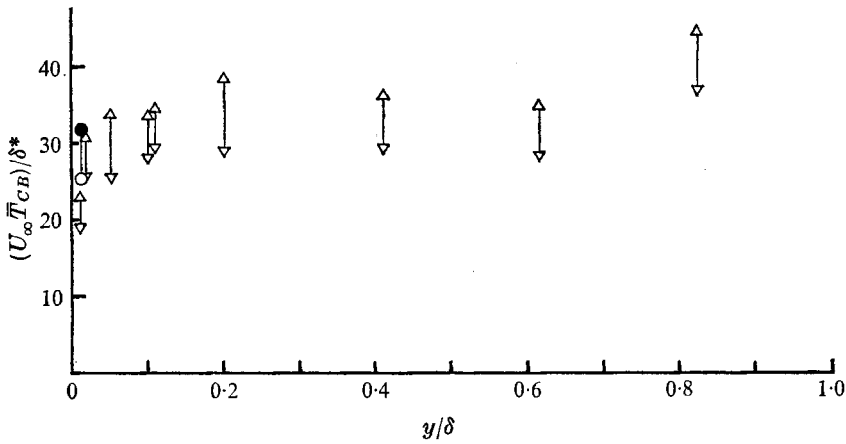
FIGURE 17. Characteristic mean time intervals between large bursts. $Re_\theta \simeq 38\,000$:
$\bullet$, $H = 4\cdot5$; $\bigcirc$, $H = 4\cdot0$. $Re_\theta \simeq 4230$: $\triangle$, $H = 4\cdot5$; ∇, $H = 4\cdot0$.

4·5, only $\widetilde{uv_2}/\overline{uv}$ is not zero regardless of the distance from the wall. Contributions to $\overline{uv}$ above this value of H must have come from the large spikes in the uv signal related to the bursts. For a hole size $H \simeq 4\cdot5$, $|uv|$ is about ten times the absolute value of the local mean Reynolds stress. These bursts certainly are very violent relative to the value of $\overline{uv}$ at a given distance from the wall. Using this unique feature, applied consistently throughout the boundary layer, one can obtain a consistent measure of the characteristic time interval $\overline{T}_{CB}$ between relatively large contributions to $\overline{uv}$ (which are larger than contributions to $\overline{uv}$ from any other quadrant at a given distance from the wall) by setting H at the specified level $H \simeq 4$–4·5.

Using this scheme, a consistent estimate of the characteristic time interval between relatively large bursts is shown in figure 17, which was obtained from figure 16 by setting $H \simeq 4$–4·5. A value of $U_\infty \overline{T}_{CB}/\delta^* \approx 32$ is found for most of the boundary layer. Measurements from the single high Reynolds number run are also included in figure 17. The fact that the value of $\overline{T}_{CB}$ determined as described above scales with the outer flow variables is in accord with the scaling of the mean period between bursts reported by Rao *et al.* (1971). It must be regarded as a coincidence that the actual value of $U_\infty \overline{T}_{CB}/\delta^* \simeq 32$ (determined with $H \simeq 4$–4·5) is almost the same as the value of the mean burst period determined by Rao *et al.* (1971). In this connexion we again mention that the method used by Rao *et al.* (1971) to obtain the value $U_\infty \overline{T}/\delta^* \simeq 30$ from the high Reynolds number data of Tu & Willmarth (1966) is not correct; see the beginning of this section.

A similar scheme was used to measure the mean time interval $\overline{T}_S$ between sweep contributions. A sweep is assumed to occur if the uv signal in the fourth quadrant reaches or exceeds a specified value. Thus, as in the case of bursts, the mean time interval $\overline{T}_S$ between sweeps is also a function of the hole size H and the mean time interval between sweeps in non-dimensional form $U_\infty \overline{T}_S/\delta^*$ is shown in figure 18 as a function of H, with y/δ as a parameter. The data are more
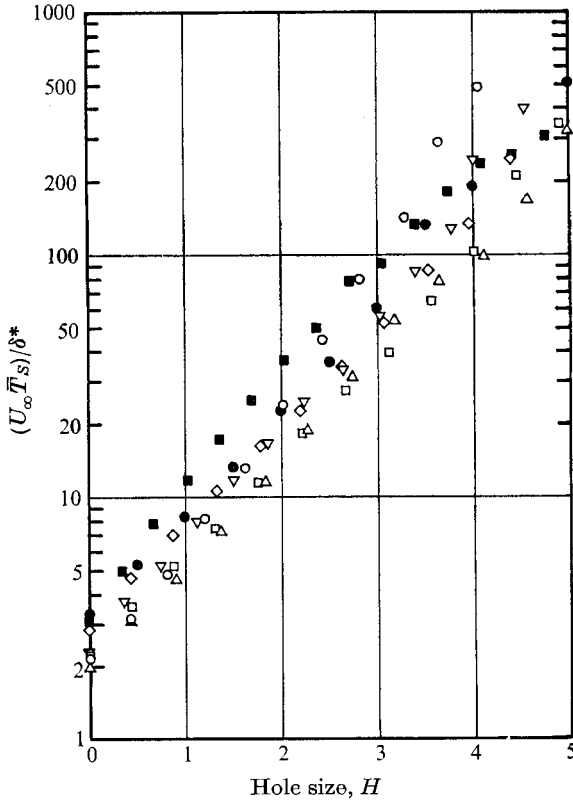
FIGURE 18. Mean time interval between sweeps as a function of hole size H and distance from wall; $Re_\theta \simeq 4230$. Symbols same as in figure 16.

scattered than those of figure 16, but the dependence of $U_\infty \overline{T}_S/\delta^*$ on the distance from the wall is not very great. As in the case of bursts, there is a no plateau in the mean time $\overline{T}_S$ between sweep contributions as H increases. Therefore, H alone cannot be used to determine the actual mean time between sweep contributions.

There is, however, another unique feature in the plots of the contributions to $\overline{uv}$ from different events (figures 11 and 12). At a hole size $H \simeq 2 \cdot 25$–$2 \cdot 75$, at any distance from the wall in the boundary layer, $\widetilde{uv}_1/\overline{uv}$ and $\widetilde{uv}_3/\overline{uv}$ vanish. Thus, the characteristic time interval $\overline{T}_{CS}$ between relatively large sweeps can be obtained by setting H at the level at $H \simeq 2 \cdot 25$–$2 \cdot 75$. When determined in this fashion, $\overline{T}_{CS}$ represents a consistent estimate of the mean time between sweeps which are larger than the largest positive contributions to $\overline{uv}$ at any given distance from the wall. Figure 19 shows the values of $U_\infty \overline{T}_{CS}/\delta^*$ obtained for H between $2 \cdot 25$ and $2 \cdot 75$ as a function of distance from the wall. A value of about 30 for $U_\infty \overline{T}_{CS}/\delta^*$ is found in most of the boundary layer. Thus, $U_\infty \overline{T}_{CB}/\delta^*$ and $U_\infty \overline{T}_{CS}/\delta^*$ are essentially equal. The same result was obtained for the high Reynolds number flow measurement. It appears that $\overline{T}_{CS}$ may also scale with the outer flow variables. Further studies of the sweep events at different Reynolds numbers and of their relationship to bursting are needed.
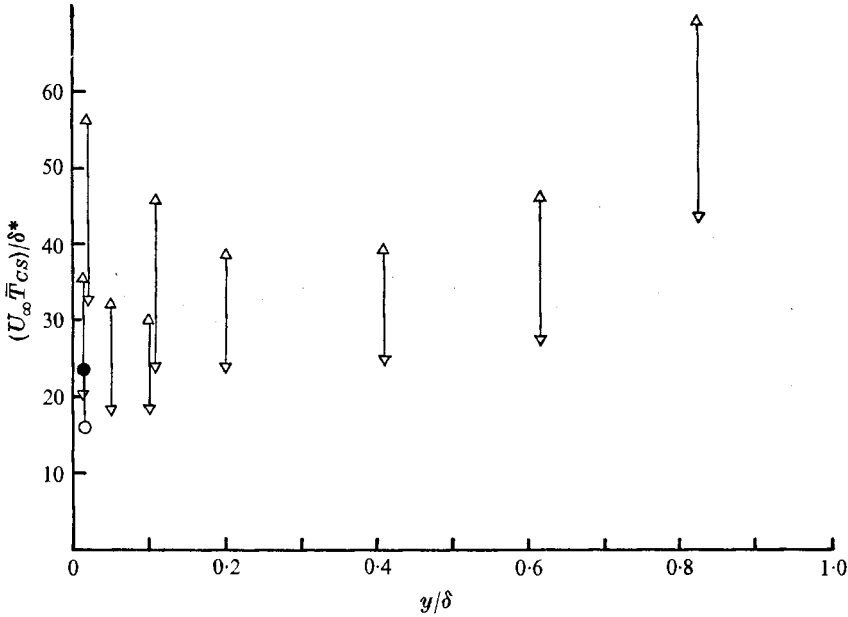
FIGURE 19. Characteristic mean time intervals between large sweeps.
Symbols same as in figure 17.

5.2. *Measurements of burst and sweep duration*

The mean time scale (or duration) of the burst was obtained by measuring the mean time during which the uv signal exceeded the specified level. In other words, the time scale $\overline{\Delta T_B}$ can be expressed as

$$\overline{\Delta T_B}(H) = \lim_{T \to \infty} \frac{1}{T} \int_0^T \Delta T_B S_2(t, H)\, dt, \tag{13}$$

where ΔT_B is the time during which the function $S_2(t, H)$ of $(10a)$ is unity.

A similar expression can be written for the mean time scale ΔT_S (or duration) of the sweep as

$$\overline{\Delta T_S}(H) = \lim_{T \to \infty} \frac{1}{T} \int_0^T \Delta T_S S_4(t, H)\, dt, \tag{14}$$

where $S_4(t, H)$ is the function in $(10a)$ and ΔT_S is the time during which $S_4(t, H)$ is unity.

Counting of the number of bursts and sweeps and the computations of $\overline{\Delta T_B}$ and $\overline{\Delta T_S}$ were accomplished as part of the same computer program as that used to determine the contributions to $\overline{uv}$ from different events.

The time scale $U_\infty \overline{\Delta T_B}/\delta^*$ of the burst in non-dimensional form is shown in figure 20 as a function of hole size for the low-speed measurements. The time scale of bursts is seen to increase as one moves away from the wall. The characteristic time scale $\overline{\Delta T_{CB}}$ for large bursts is shown figure 21, which was obtained from figure 20 by setting $H \simeq 4$–$4 \cdot 5$. The single measurement for high Reynolds number flow gave a value of $0 \cdot 21$, which is somewhat small compared with that
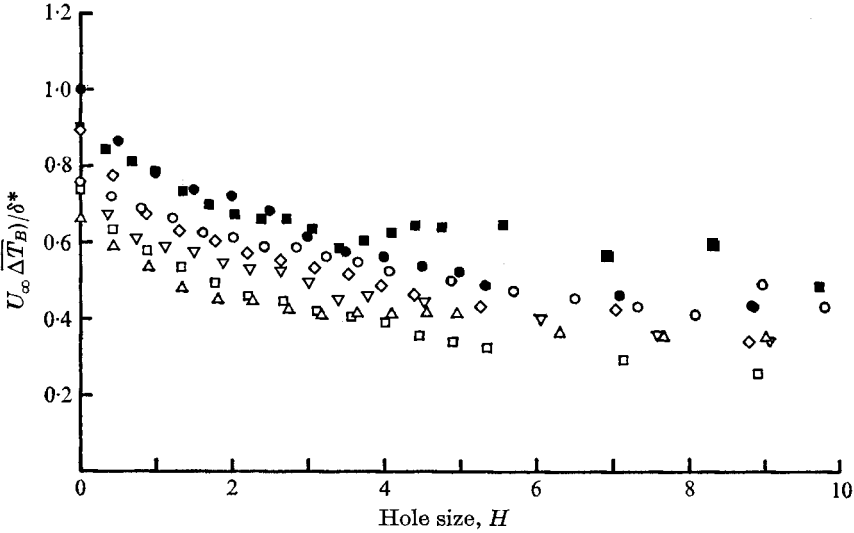
FIGURE 20. Mean duration of bursts as a function of hole size H and distance from the wall; $Re_\theta \simeq 4230$. Symbols same as in figure 16.
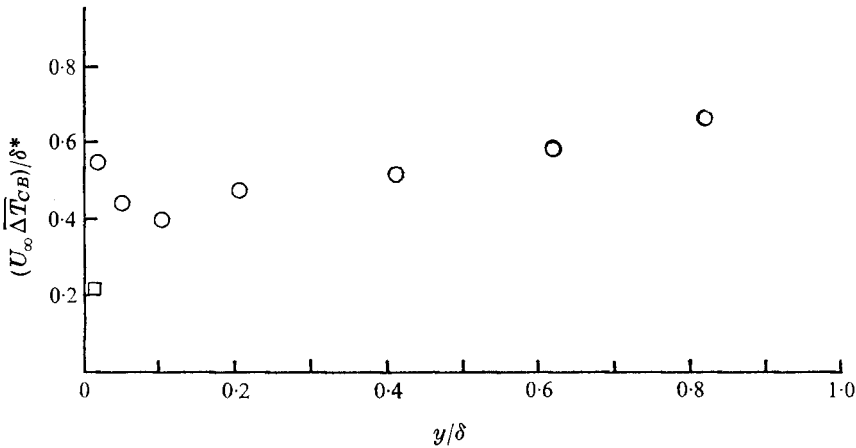

FIGURE 21. Characteristic mean duration of large bursts measured as a function of y/δ. O, Re_θ 4230; □, $Re_\theta \simeq 38000$.

for low-speed measurements. The time scale of the sweep is shown in figure 22. The general trend that the time scale increases as the distance from the wall increases is also observed. Figure 23 shows the characteristic time scale $\overline{\Delta T}_{CS}$ for large sweeps. This figure was obtained by setting $H \simeq 2 \cdot 25 – 2 \cdot 75$. A lower value of $0 \cdot 16$ for $U_\infty \overline{\Delta T}_{CS}/\delta^*$ was obtained for the high-speed measurement. At constant y/δ, the variation of the time scales $\overline{\Delta T}_{CB}$ and $\overline{\Delta T}_{CS}$ with H (figures 20 and 22) is very much smaller than the variation of the average burst and sweep time intervals $\overline{T}_B$ and $\overline{T}_S$ (figures 15 and 18). This indicates that periods of burst or sweep activity have on average approximately the same duration regardless of whether the contribution to the local Reynolds stress during the active period is large (and infrequent) or small (and more frequent).
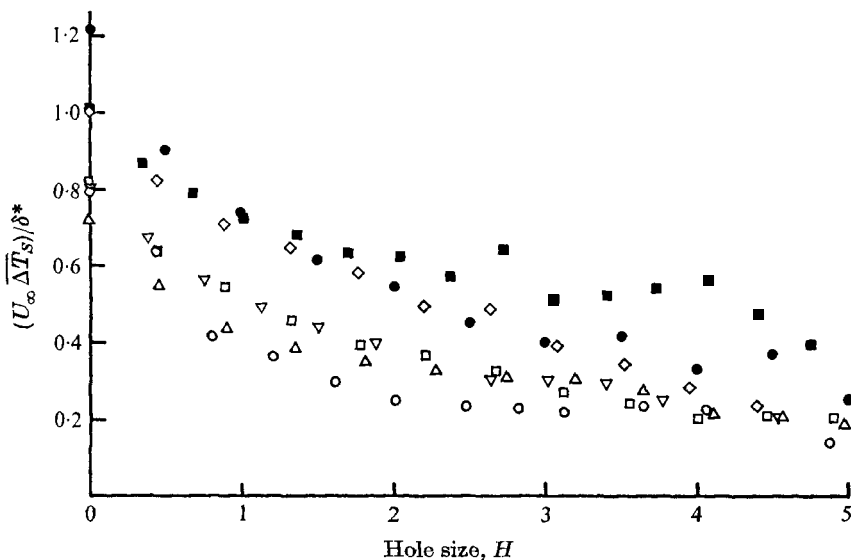
FIGURE 22. Mean duration of sweeps as a function of hole size H and distance from the wall; $Re_\theta \simeq 4230$. Symbols same as in figure 16.
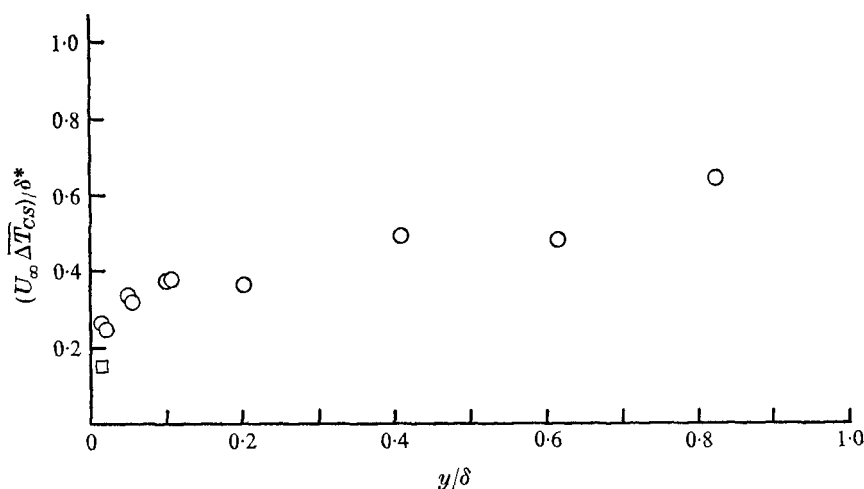

FIGURE 23. Characteristic mean duration of large sweeps measured as a function of y/δ. Symbols same as in figure 21.

6. Discussion of measurements

The ejection of low-momentum fluid from the wall is a dominant feature of the structure of the turbulent boundary layer. The importance of the ejection or burst is obvious from the study of the ratio $\widetilde{uv}_2/\widetilde{uv}_4$ at $H = 0$. Near the wall, the ratio is the highest with a value of 1·8, while in the outer region a smaller value of 1·35 is obtained (see figure 14). Thus, the ejection is more violent near the wall as was better illustrated by the measurements of Willmarth & Lu (1971), in

which very large individual contributions to $\overline{uv}$ ($uv \simeq 62\overline{uv}$) where identified near the wall.

The violent burst events near the wall were studied in §3. Conditionally sampled measurements of $\langle uv_2 \rangle$ show that near the wall the various portions of the deterministic burst pattern are convected at somewhat less than the local mean speed (i.e. at $y \simeq 0.15\,\delta^*U_{CB}/U \simeq 0.8$). As the deterministic burst pattern is convected downstream it enlarges both spanwise and in a direction normal to the wall. However, the rate of convection is much greater than the transverse rate of growth. For example, no contributions to $\langle uv_2 \rangle$ can be measured when the X-wire probe is far downstream of the detector probe and a line between the X-probe and detector probe forms an angle greater than approximately $10°$ with the stream direction. In addition, the contributions to $\langle uv_2 \rangle$ decay as one moves the X-wire probe downstream at a constant small distance from the wall.

There is no doubt that these measurements indicate that an initially small deterministic burst pattern is growing in scale and is distorted by the shearing motion as it is convected downstream. The question of how large the evolving, deterministic bursting patterns ultimately become cannot definitely be answered until someone devises (if it is possible) a more reliable burst detection scheme. It seems likely that the effects of a violent ejection near the wall can, after evolution and convection, reach a station remote from the wall in the turbulent boundary layer. This conjecture is in agreement with the results of Grass (1971), the speculations of Kovasznay *et al.* (1970) and present results, which show that $\overline{T}_{CB}$ is approximately constant throughout the boundary layer.

Although definitive identification of bursts and sweeps is difficult some characteristic mean time intervals between bursts and sweeps have been found. The scaling of the mean time interval $\overline{T}_{CB}$ between large bursts with the outer flow variables at Reynolds numbers Re_θ of 4230 and 38000 is confirmed. As for the large sweeps, the mean sweep rates were also obtained for the Reynolds numbers Re_θ of 4230 and 38000. The mean time interval between sweeps is roughly the same as that between bursts. There is not enough data to allow us to draw a firm conclusion about the scaling of the sweep rate, although at both Reynolds numbers we obtain roughly the same value of about 30 for $U_\infty \overline{T}_{CS}/\delta^*$ using the methods of §5. However, if large bursting events are indeed followed by large sweeps as suggested by Corino & Brodkey (1969),[†] the mean sweep period must also scale with the outer flow parameters and $U_\infty \overline{T}_{CS}/\delta^* \approx U_\infty \overline{T}_{CB}/\delta^* \approx 32$.

The contributions to $\overline{uv}$ from the bursts is about 77 % throughout the boundary layer, for $y > 0.05\delta^*$, which is in essential agreement with the measurements of others (e.g. Kim *et al* 1968; Corino & Brodkey 1969; Grass 1971; etc.). However, Wallace *et al.* (1972) reported a larger contribution to $\overline{uv}$ from the sweeps near the wall, $y^+ < 15$, in a channel flow (see figure 15). The reason for this discrepancy has not been determined, but may be caused by the flow geometry; all the other measurements were made in boundary layers. At any rate, the scaling of the burst rate with outer flow variables and the scaling of $(\widetilde{uv}_2/\widetilde{uv}_4)_{H=0}$ (see figure 15) with inner flow variables suggest that the occurrence of bursts is determined by

[†] Offen & Kline, in a recent paper submitted to the *Journal of Fluid Mechanics*, have concluded from visual studies that bursts and sweeps *sometimes* form a cycle in space and time.

the outer flow conditions while the ensuing events near the wall after the burst begins are related to the wall-region variables.

It has been speculated that the bursts may have some bearing on the turbulent 'bulges' in the outer intermittent flow region (see, for example, Kovasznay *et al.* 1970; Laufer & Badri Narayanan 1971). The present measurements of the mean time interval between bursts seem to confirm this idea. The mean burst period $\overline{T}_{CB}$ is approximately constant for most of the boundary layer while the time scale $\overline{\Delta T}_{CB}$ increases with increasing distance from the wall. This suggests that after a burst originates near the wall it evolves into a larger convected disturbance with an unchanged time interval $\overline{T}_{CB}$ between bursts but a larger time scale $\overline{\Delta T}_{CB}$. In addition, our measurements of contributions to $\overline{uv}$ from different events as a function of H (figures 11, 12) show that the contributions $\widetilde{uv}_i$ $(u = 1, \ldots 4, h)$ are very similar throughout the boundary layer. This again is consistent with the idea that the bursting events originating near the wall continue to produce, as they evolve, relatively the same (but larger scale and less intense) contributions to $\widetilde{uv}_i$ throughout the boundary layer.

The dominant feature of ejection in a turbulent boundary layer can be seen in the plots of contributions to $\overline{uv}$ from different events (figures 11, 12). Besides this, other statistical characteristics of the uv signal are fairly predictable from the assumption of joint-normality for u and v signals except very close to the wall ($y^+ < 90$) and in the outer intermittent region. These facts lead one to speculate that the turbulence in the inner part of the turbulent boundary layer may be considered as a 'universal motion' plus an 'irrelevant motion' as suggested by Townsend (1957, 1961). The 'universal motion' may be considered as random occurrence (both temporally and spatially) of bursts, which is controlled by the outer flow, plus the ensuing more diffuse return flow, which may be related to the sweeps. The 'irrelevant motion' may be considered as the accumulation of the remnants of what has happened upstream. The contribution to $\overline{uv}$ from the latter would be small.

From the measurements of sampled Reynolds stress $\langle uv \rangle$ near the wall using the sampling criteria that the velocity u_w at the edge of the viscous sublayer be low and decreasing, it is found that there are bursts producing large contributions to the Reynolds stress that are convected at speeds lower than the local mean speed. In addition the line in the x, y plane on which the peak values of $\langle uv \rangle$ occur, with no time delay, travels outwards from the wall at an angle of 16°–20°. This may be explained by the convection past the measuring station of a certain deterministic pattern, for example, the hairpin vorticity model proposed by Willmarth & Tu (1967). This model was suggested and is consistent with the numerous space–time correlation measurements reported by Willmarth & Wooldridge (1962, 1966) and Tu & Willmarth (1966). As a matter of fact, this pattern of vorticity, if imagined to evolve to a larger scale, may also be used to describe the time sequence of the instantaneous velocity profiles near the wall as observed by Kim *et al.* (1968, figure 4.13) and could produce intermittent turbulent bulges at the outer edge of the boundary layer. This would provide the interaction between the inner and outer regions of the boundary layer that is implied by the scaling of the mean time between bursts with the outer flow

variables. Since a large part of the Reynolds stress near the wall is produced during the times when our sampling procedure indicates that bursts occur, it is likely that a model like that of Willmarth & Tu (1967) may determine the flow structure near the wall and may well be a part of the 'universal motion' mentioned above.

REFERENCES

BLACKWELDER, R. F. & KAPLAN, R. E. 1971 Intermittent structure in turbulent boundary layers. *NATO–AGARD Conf. Proc. on Turbulent Shear Flow*, no. 93, p. 5.

COANTIC, M. 1965 *Comptes Rendus*, **260**, 2981.

CORINO, E. R. & BRODKEY, R. S. 1969 *J. Fluid Mech.* **37**, 1.

ECKELMANN, H. 1970 *Mitteilungen MPI fur Stromungsforschung und der AVA, Göttingen*, no. 48.

GRASS, A. J. 1971 *J. Fluid Mech.* **50**, 2, 233.

GUPTA, A. K. & KAPLAN, R. E. 1972 *Phys. Fluids*, **15**, 981.

KIBENS, V. 1968 The intermittent region of a turbulent boundary layer. Ph.D. dissertation, The Johns Hopkins University.

KIM, H. T., KLINE, S. J. & REYNOLDS, W. C. 1968 An experimental study of turbulence production near a smooth wall in a turbulent boundary layer with zero pressure gradient. *Thermosciences Division, Mech. Engng Dept., Stanford University Rep.* MD-20.

KIM, H. T., KLINE, S. J. & REYNOLDS, W. C. 1971 *J. Fluid Mech.* **50**, 133.

KLEBANOFF, P. S. 1954 Characteristics of turbulence in a boundary layer with zero pressure gradient. *N.A.C.A. Tech. Note*, no. 3178.

KLINE, S. J., REYNOLDS, W. C., SCHRAUB, F. A. & RUNSTADLER, P. W. 1967 *J. Fluid Mech.* **30**, 741.

KOVASZNAY, L. S. G., KIBENS, V. & BLACKWELDER, R. F. 1970 *J. Fluid Mech.* **41**, 283.

LAUFER, J. 1953 The structure of turbulence in a fully developed pipe flow. *N.A.C.A. Tech. Note*, no. 2954.

LAUFER, J. & BADRI NARAYANAN, M. A. 1971 *Phys. Fluids*, **14**, 182.

LU, S. S. & WILLMARTH, W. W. 1972 The structure of the Reynolds stress in a turbulent boundary layer, *Dept. Aerospace Engng, University of Michigan, ORA Rep.* 021490-2-T.

LU, S. S. & WILLMARTH, W. W. 1973 *Phys. Fluids.* **16**, to appear.

RAO, K. N., NARASIMHA, R. & BADRI NARAYANAN, M. A. 1969 Hot-wire measurements of burst parameter in a turbulent boundary layer. *Dept. of Aeron. Engng, Indian Institute of Science, Bangalore. Rep.* no. 69 FM 8.

RAO, K. N., NARASIMHA, R. & BADRI NARAYANAN, M. A. 1971 *J. Fluid Mech.* **48**, 339.

REICHARDT, H. 1938 Messungun turbulenter Schwangkungen, *Naturwiss.* **26**, 404.

RUNSTADLER, P. W., KLINE, S. J. & REYNOLDS, W. C. 1963 An investigation of the flow structure of the turbulent boundary layer. *Thermosciences Division, Mech. Engng Dept., Stanford University Rep.* MD-8.

SCHRAUB, F. A. & KLINE, S. J. 1965 Study of the structure of the turbulent boundary layer with and without longitudinal pressure gradients. *Thermosciences Division, Mech. Engng Dept., Stanford University Rep.* MD-12.

TOWNSEND, A. A. 1951 *Proc. Camb. Phil. Soc.* **47**, 375.

TOWNSEND, A. A. 1957 The turbulent boundary layer. *IUTAM. Symp. Freiburg*, pp. 1–15. Springer.

TOWNSEND, A. A. 1961 *J. Fluid Mech.* **11**, 97.

TRITTON, D. J. 1967 *J. Fluid Mech.* **28**, 439.

TU, B. J. & WILLMARTH, W. W. 1966 An experimental study of the structure of turbulence near the wall through correlation measurements in a thick turbulent boundary layer. *University of Michigan Tech. Rep.* ORA 02920-3-T.

WALLACE, J. M., ECKELMANN, H. & BRODKEY, R. S. 1972 *J. Fluid Mech.* **54**, 39.

WILLMARTH, W. W. & LU, S. S. 1971 Structure of the Reynolds stress near the wall. *AGARD Conf. Proc. on Turbulent shear Flow*, no. 92, p. 3. (See also 1972 *J. Fluid Mech.* **55**, 65.)

WILLMARTH, W. W. & TU, B. J. 1967 *Phys. Fluids*, **10**, S 134.

WILLMARTH, W. W. & WOOLDRIDGE, C. E. 1962 *J. Fluid Mech.* **14**, 187.

WILLMARTH, W. W. & WOOLDRIDGE, C. E. 1966 *AGARD–NATO Rep.* no. 456.

ZARIC, Z. 1972 *Comptes Rendus*, A **275**, 513.